![IGS logo]

Article

Corresponding author:
Aleah Sommers;
Email: Aleah.N.Sommers@dartmouth.edu

Subglacial hydrology modeling predicts high winter water pressure and spatially variable transmissivity at Helheim Glacier, Greenland

Aleah Sommers[1] , Colin Meyer[1], Mathieu Morlighem[1] , Harihar Rajaram[2], Kristin Poinar[3] , Winnie Chu[4] and Jessica Mejia[3]

[1]Dartmouth College, Hanover, NH, USA; [2]Johns Hopkins University, Baltimore, MD, USA; [3]University at Buffalo, Buffalo, NY, USA; and [4]Georgia Institute of Technology, Atlanta, GA, USA

Abstract

Water pressure beneath glaciers influences ice velocity. Subglacial hydrology models are helpful for gaining insight into basal conditions, but models depend on unconstrained parameters, and a current challenge is reproducing elevated water pressures in winter. We eliminate terms related to englacial storage, opening by sliding, and melt due to changes in the pressure-melting-point temperature, to create a minimalist version of the Subglacial Hydrology And Kinetic, Transient Interactions (SHAKTI) model, and apply this model to Helheim Glacier in east Greenland to explore the winter base state of the subglacial drainage system. Our results suggest that meltwater produced at the bed alone supports active winter drainage with large areas of elevated water pressure and preferential drainage pathways, using a continuum approach that allows for transitions between flow regimes. Transmissivity varies spatially over several orders of magnitude from 10^{-4} to 10^3 m^{2}s^{-1}, with regions of weak transmissivity representing poorly connected regions of the system. Bed topography controls the location of primary drainage pathways, and high basal melt rates occur along the steep valley walls. Frictional heat from sliding is a dominant source of basal melt; different approaches for calculating basal shear stress produce significantly different basal melt rates and subglacial discharge.

1. Introduction

Conditions at the beds of ice sheets and glaciers strongly influence ice dynamics through the effect of lubrication and enhanced sliding where basal water pressure is high. Unfortunately, direct observations are difficult to obtain beneath hundreds to thousands of meters of ice. Techniques such as drilling boreholes to the bed (Iken and others, 1993; Murray and Clarke, 1995; Harper and others, 2005; Fudge and others, 2008; Andrews and others, 2014; Ryser and others, 2014), using radar sounding to infer the presence of liquid basal water (Oswald and Gogineni, 2008; Chu and others, 2016; Jordan and others, 1999; Oswald and others, 2018), and dye-tracing tests (Nienow and others, 1998; Cowton and others, 2013) are helpful means to gain a view into basal conditions, but do not provide a complete description of the spatially and temporally heterogeneous bed environment.

Several numerical models have been developed to simulate the flow and pressure of water beneath glaciers and ice sheets (e.g., Flowers, 2015; de Fleurian and others, 2018) and have successfully reproduced melt-season drainage system evolution. However, challenges remain in these efforts, and subglacial hydrology model development remains an active area of research. One persistent issue is that many models rely on unconstrained parameters, for example, prescribing a typical height and spacing of asperities at the bed, or specifying hydraulic conductivity of drainage system components. Subglacial hydrology models are sensitive to these uncertain parameters, with small changes leading to substantial differences in simulated basal water pressures and drainage regimes (Werder and others, 2013; Banwell and others, 2016).

Another challenge is that models have had difficulty reproducing widespread areas of high winter water pressures (Flowers, 2015) that have been observed in Greenland borehole arrays (Harper and others, 2005; Ryser and others, 2014). Recent work highlighting the importance of hydraulically disconnected regions of the bed and incorporating a representation of these isolated areas into drainage models has helped to explain this phenomenon (Hoffman and others, 2016; Rada and Schoof, 2018; Rada Giacaman and Schoof, 2023), linking disconnected regions with other drainage components that represent flow through inefficient sheet-like configurations and efficient channels. Different drainage 'modes' are treated with disparate equations to represent distinct physical processes (for example, channels open by melting while the sheet-like system opens by sliding over asperities in the bed). However, distinguishing between drainage modes by applying separate equations to represent different components imposes an artificial distinction and may fail to fully capture the continuous spectrum of spatio-temporally evolving drainage behavior that exists in reality. In addition, much of the previous work modeling subglacial hydrology in Greenland focuses on land-terminating glaciers in west Greenland. Although recent modeling efforts have been applied to Greenland tidewater glaciers such as Store Glacier (Cook and others, 2020, 2022), Petermann Glacier (Ehrenfeucht and others, 2023), and Helheim Glacier (Stevens and others, 2022), not as much attention

![CrossMark logo]

has been directed at tidewater glaciers in this context, despite their outsize influence on mass loss from the ice sheet.

In this paper, we describe a reduced form of the Subglacial Hydrology And Kinetic, Transient Interactions (SHAKTI) model to address the above-mentioned issues. First presented by Sommers and others (2018), SHAKTI takes a continuum approach without explicitly distinguishing between different drainage components, yet does represent behavior corresponding to different 'modes' of drainage, primarily facilitated through flow regime transitions with a single set of equations. Here, we eliminate some terms that rely on unconstrained parameters or uncertain physics, and which are not needed in order to obtain a minimal model. After summarizing the equations governing the evolution of the subglacial hydrology system in SHAKTI, we apply the model to Helheim Glacier in east Greenland under winter conditions to demonstrate its capabilities in a real glacial setting and attempt to reconcile the outstanding problem of simulating high winter water pressures with a continuum model. We also examine the role of basal melt from frictional heat and the influence of different styles of calculating basal shear stress.

2. Methods

2.1 Summary of equations

SHAKTI uses a single set of equations to calculate hydraulic head, effective pressure, basal water flux, and geometry of the subglacial drainage system. In contrast to other subglacial hydrology models, SHAKTI allows for natural transitions between laminar and turbulent flow, allowing distinct flow regimes to coexist in different regions of the model domain with spatially and temporally variable transmissivity, giving rise to a spectrum of inefficient and efficient drainage configurations. SHAKTI includes heat generated by energy dissipation within the water flow and opening of the drainage system by melt across the entire domain, unlike models that treat 'inefficient' sheet-like and 'efficient' channel-like components of the drainage system with different equations. SHAKTI's unified approach leads to the emergence and disappearance of flexible drainage configurations over time, conserving mass and energy within the system. In what follows, we summarize the original SHAKTI model equations, along with key modifications to eliminate terms that depend on unconstrained parameters. Whereas in the original SHAKTI formulation, we included terms to facilitate direct comparison to other models (de Fleurian and others, 2018), here we examine the model capabilities in the absence of these unconstrained terms. Tables 1 and 2 serve as convenient references for the variables, constants, and parameters used in the equations. For a complete description of the original SHAKTI model, we refer readers to Sommers and others (2018).

SHAKTI is composed of partial differential equations that describe conservation of ice and water mass, drainage configuration, water flux, and internal melt generation. The water balance equation is written as

$$\frac{\partial b}{\partial t} + \frac{\partial b_e}{\partial t} + \nabla \cdot \mathbf{q} = \frac{\dot{m}}{\rho_w} + i_{e \to b}, \qquad (1)$$

where b is the gap height between the ice and bed, b_e refers to a volume of water stored englacially per unit area of the bed, $\mathbf{q}$ is gap-integrated water flux through the subglacial system, $\dot{m}$ is the melt rate expressed as a mass flux (units of kg m^{-2} s^{-1}), ρ_w is density of water, and $i_{e \to b}$ is the rate of meltwater input from the englacial system to the bed, which can be specified and handled by the model as a combination of distributed input

Table 1. Variables

Symbol	Units	Description
b	m	Gap height
b_e	m	Englacial storage per unit area of bed
h	m	Hydraulic head
K	m^2 s^{-1}	Hydraulic transmissivity, $K = b^3 g/(12\nu(1 + \omega Re))$
$\dot{m}$	kg m^{-2} s^{-1}	Subglacial melt rate
N	Pa	Effective pressure, $N = p_i - p_w$
p_i	Pa	Ice overburden pressure, $p_i = \rho_i gH$
p_w	Pa	Water pressure, $p_w = \rho_w g(h - z_b)$
$\mathbf{q}$	m^2 s^{-1}	Water flux
Re	Dimensionless	Reynolds number, Re$=|q|/\nu$
t	s	Time
β	Dimensionless	Parameter controlling opening due to sliding over bed bumps, $\beta = (b_r - b)/l_r$ for $b < b_r$, $\beta = 0$ for $\beta \geq b_r$
τ_b	Pa	Basal stress

(units of m s^{-1}) and point inputs to represent moulins or crevasses (units of m^3 s^{-1}).

For our current purposes of simulating a steady-state minimal winter base state, the term $\frac{\partial b_e}{\partial t}$ is zero. This implies that all simulated water is at the bed and we do not attempt to approximate delayed release from englacial storage, although water held in void spaces within the ice could play an important role in subglacial water flow even in the absence of surface melt (Schoof and others, 2014). For winter conditions, with no englacial storage and no external meltwater inputs, the modified water balance equation is then given by

$$\frac{\partial b}{\partial t} + \nabla \cdot \mathbf{q} = \frac{\dot{m}}{\rho_w}. \qquad (2)$$

The geometry of the drainage system is represented by the average gap height b over a discrete area of the bed, which evolves through time dynamically. In the original equations, gap height increases as a result of both melt and by sliding over bumps in the bed, and decreases due to creep deformation. This can be expressed as change in gap height over time as

$$\frac{\partial b}{\partial t} = \frac{\dot{m}}{\rho_i} + \beta|\mathbf{u}_b| - A|p_i - p_w|^{n-1}(p_i - p_w)b, \qquad (3)$$

where ρ_i is the density of ice, β is a dimensionless coefficient that dictates opening of the subglacial gap by sliding over bumps in the bed, $\mathbf{u}_b$ is the ice sliding velocity, A is the flow law parameter, $p_i = \rho_i g H$ is ice overburden pressure in which g is gravitational acceleration and H is ice thickness, $p_w = \rho_w g (h - z_b)$ is subglacial water pressure in which h is hydraulic head and z_b is bed elevation above sea level, and n is Glen's flow law exponent.

The coefficient β that governs opening by sliding over bumps in the bed depends on prescribing an uncertain 'typical bed-bump height' (b_r) and 'typical bed-bump spacing' (l_r), following Werder and others (2013). This method of cavity opening was introduced by Hewitt (2011) to parameterize an opening mechanism in distributed drainage other than melt, based on the description of linked cavities of Kamb (1987). Schoof and others (2012) found that a system of linked cavities that opened by melt was unstable (assuming turbulent flow); therefore, the opening-by-sliding mechanism has been widely adopted for the evolution of inefficient drainage systems. However, to prevent numerical instability in other models that use this type of opening mechanism, sliding velocity must usually be capped. For example, Poinar and others

Table 2. Constants and parameters used in this study

Symbol	Value	Units	Description
A	2.4×10^{-24}	Pa^{-3} s^{-1}	Flow law parameter (for ice at 0° Celsius)
b_r	0	m	Typical height of bed bumps
C	Spatially varying	s$^{1/2}$ m$^{-1/2}$	Drag coefficient used in basal stress calculation
c_t	7.5×10^{-8}	K Pa^{-1}	Change of pressure melting point with temperature
c_w	4.22×10^3	J kg^{-1} K^{-1}	Heat capacity of water
G	0.05	W m^{-2}	Geothermal flux (Martos and others, 2018)
g	9.81	m s^{-2}	Gravitational acceleration
H	Varying	m	Ice thickness (Morlighem and others, 2017)
$i_{e \to b}$	0	m s^{-1} or m^3 s^{-1}	Input rate of meltwater to subglacial system
L	3.34×10^5	J kg^{-1}	Latent heat of fusion of water
l_r	0	m	Typical spacing between bed bumps
μ	0.3	Dimensionless	Till coefficient used in yield stress
n	3	Dimensionless	Flow law exponent
$\mathbf{u}_b$	Varying	m s^{-1}	Ice velocity (Joughin and others, 2018)
z_b	Varying	m	Bed elevation with respect to sea level
ν	1.787×10^{-6}	m^2 s^{-1}	Kinematic viscosity of water
ω	0.001	Dimensionless	Parameter controlling nonlinear laminar/turbulent transition
ρ_i	917	kg m^{-3}	Bulk density of ice
ρ_w	1000	kg m^{-3}	Bulk density of water

(2019) applied the Glacier Drainage System model (GlaDS) (Werder and others, 2013) with $b_r = 0.08$ m and $l_r = 2$ m to an idealized Helheim Glacier-like domain, and had to cap sliding speed at 800 m yr^{-1} to achieve model stability. This is an order of magnitude less than observed velocity on Helheim Glacier. Stevens and others (2022) used a similar model to simulate subglacial hydrology at Helheim and chose a bed bump height of 0.1 m and spacing of 10 m without imposing a limit on the velocity, but did not address sensitivity of the resulting subglacial drainage system to these choices of bed roughness geometry. Applying GlaDS to Sermeq Kujalleq (Store Glacier), a tidewater glacier in west Greenland, Cook and others (2020, 2022) selected higher bed bump and spacing values, $b_r = 1$ m and $l_r = 100$ m. In fast-flowing glaciers, we find that including opening by sliding over bumps in SHAKTI effectively smooths out and inhibits any channelized structure, leading to an unrealistic near-uniform gap height equal to the specified bed bump height over large regions. This opening mechanism was included in the original SHAKTI equations largely for comparison with other similar models, but is not required for model stability due to the transitional flux formulation that allows for changes between laminar and turbulent flow regimes, discussed below in Equation (5) and by Sommers and others (2018).

Given how the opening-by-sliding parameterization depends on arbitrarily prescribed bed-bump height and spacing that in reality are heterogeneous, we cannot be confident that the commonly used formulation accurately represents the increase in average b – especially in the case of fast-flowing glaciers, which we expect to be underlain by till. We eliminate the 'opening by sliding over bumps at the bed' term $\beta |\mathbf{u}_b|$ and allow the drainage geometry to open only due to melt, everywhere in the domain, which behaves stably with our transitional flux formulation (Eqn. (5) below). The minimum gap height allowed is 10^{-3} m, representing a transition to premelted films (Wettlaufer and Worster, 2006; Rempel and others, 2022). We write our modified basal gap dynamics equation as

$$\frac{\partial b}{\partial t} = \frac{\dot{m}}{\rho_i} - A |p_i - p_w|^{n-1} (p_i - p_w) b. \tag{4}$$

The momentum equation that describes the water flux is

$$\mathbf{q} = \frac{-b^3 g}{12\nu(1 + \omega Re)} \nabla h, \tag{5}$$

where ν is kinematic viscosity of water, ω is a parameter related to a friction factor that controls the transition from laminar to turbulent flow, and $Re = |\mathbf{q}|/\nu$ is the local Reynolds number. When $\omega Re \ll 1$, Eqn. (5) behaves like laminar flow, with $\mathbf{q}$ proportional to the magnitude of the hydraulic gradient $|\nabla h|$. When $\omega Re \gg 1$, by inserting the definition Re and rearranging to solve for $\mathbf{q}$, we see that $\mathbf{q}$ is proportional to $\sqrt{|\nabla h|}$, corresponding to completely turbulent flow. This flux formulation is based on equations developed in the context of flow in rock fractures (Zimmerman and others, 2004; Chaudhuri and others, 2013; Rajaram and others, 2009). The general Eqn. (5) also allows for intermediate transitional regimes. This flux formulation or 'flow law' is the key difference of the original SHAKTI model compared to other subglacial hydrology models, and plays an important role in maintaining stability while allowing for channelization to occur. Forcing $\mathbf{q}$ to be always laminar or always turbulent (by changing the value of ω) results in a model instability in some situations, but these scenarios behave well when allowing for the flexible flow regime transition around $Re = 10^3$ ($\omega = 0.001$), accordingly generating spatially variable Re distributions (Sommers and others, 2018).

In contrast to models that rely on a prescribed hydraulic conductivity, this flux formulation incorporates a spatio-temporally variable hydraulic transmissivity K, given by

$$K = \frac{b^3 g}{12\nu(1 + \omega Re)}. \tag{6}$$

Basal meltwater generation is represented in SHAKTI through an energy balance at the bed, assuming ice and water are both always at the pressure melting point, i.e.

$$\dot{m}L = G + |\mathbf{u}_b \cdot \tau_b| - \rho_w g \, \mathbf{q} \cdot \nabla h + c_t c_w \rho_w \mathbf{q} \cdot \nabla p_w, \tag{7}$$

where L is the latent heat of fusion of water, G is geothermal heat flux, τ_b is the basal stress, c_t is the change of pressure melting point temperature with pressure, and c_w is the heat capacity of water. This energy equation includes melt due to heat contributed by geothermal sources, frictional heat from sliding over the bed, turbulent dissipation, and adjustments for changes in the pressure melting point due to changes in water pressure. Geothermal flux varies spatially, and the value we use here (see Table 2) corresponds to the lower-end estimate of values typical for Greenland (Martos and others, 2018). Note that Equation (9) in

Sommers and others (2018) should have a positive sign for the last term as written here in Equation (7), which accounts for changes in the sensible heat due to changes in the pressure-melting-point temperature with changes in water pressure. This term is generally a modest heat sink for flat beds, reducing the melt rate as in Röthlisberger (1972), but can also contribute to enhanced melt with steep slopes or supercooling when flowing uphill in bed overdeepenings (see, e.g. Creyts and Clarke, 2010). In regions of the bed where ice is separated from the bed by a thin film, however, the difference between ice normal stress and water pressure will be balanced by premelting, where the relationship between pressure and temperature does not follow the Clapeyron slope (Rempel and Meyer, 2019). Co-located observations of pressure and temperature within subglacial boreholes show that the Clapeyron relationship does not always hold (Huss and others, 2007). We eliminate this term for now in the reduced SHAKTI model, and leave further evaluation of the effects of pressure melting on subglacial hydrology to future work.

Basal shear stress as implemented here depends on a drag coefficient C, effective pressure N, and sliding velocity $\mathbf{u_b}$, $\tau_b = C^2 N |\mathbf{u_b}|$ (Budd and others, 1979). We use observed surface velocity as a proxy for basal sliding velocity, a reasonable assumption in fast-flowing glaciers. We also examine results using other formulations for τ_b to explore the impact of how frictional heat from sliding is represented.

The melt rate at the bed considered here in the reduced form of SHAKTI is a result of geothermal flux, frictional heat from sliding, and heat generated by mechanical energy dissipation in the subglacial system:

$$\dot{m}L = G + |\mathbf{u}_b \cdot \tau_b| - \rho_w g \, \mathbf{q} \cdot \nabla h. \tag{8}$$

We combine equations (2), (4), (5), (6), and (8) to form an elliptic equation in terms of hydraulic head:

$$\nabla \cdot (-K\nabla h) = \dot{m}\left(\frac{1}{\rho_w} - \frac{1}{\rho_i}\right) + A|p_i - p_w|^{n-1}(p_i - p_w)b. \tag{9}$$

We solve Eqn. (9) for the head distribution using a Picard iteration to handle the nonlinear dependence of the terms on the right-hand side of the equation, then we solve Eqn. (4) explicitly to evolve the gap height b. No numerical limits are imposed on head (i.e., water pressure is free to exceed overburden pressure or to become negative over the course of a simulation).

SHAKTI is built into the Ice-sheet and Sea-level System Model (ISSM; Larour and others, 2012) using the finite element method in a parallelized computational framework. In addition to the elimination of terms that rely on uncertain parameters, we modify how the term that describes creep closure in Equation (9) is handled within the Picard iteration. This change helps the Picard iteration converge instead of oscillating, a problem that arises under thick ice with low meltwater input. In previous work with SHAKTI (de Fleurian and others, 2018; Sommers, 2018), this oscillation obstacle was handled using under-relaxation. With a Newton linearization weighting, inspired by Gagliardini and Werder (2018) in their implementation of a similar subglacial hydrology model, GlaDS (Werder and others, 2013) in a different ice-sheet model, Elmer/Ice (Gagliardini and others, 2013), this change to the creep term numerics facilitates convergence of the iterative process to find h. This is a key practical improvement for the application of SHAKTI to glacial environments with thick ice and low water inputs, common in Greenland during the winter.

2.2 Model domain

We explore the winter base-state subglacial drainage of Helheim Glacier in east Greenland (Fig. 1). Helheim is a large, fast-flowing glacier that terminates in Sermilik Fjord with two main branches that flow through deeply incised canyons. We use bed and ice surface elevation based on BedMachine (Morlighem and others, 2017). Our model domain includes the two main branches of Helheim Glacier and extends inland to approximately 1900 m surface elevation. Other recent work simulating subglacial hydrology at Helheim by Stevens and others (2022) explored a smaller domain focused near the terminus region, including the smaller tributary to the north, and found the small north tributary to be relatively insignificant in winter. Our domain is discretized into an unstructured triangular mesh refined based on ice velocity, with 12472 finite elements and 6,371 vertices (Fig. S1). The area of each element ranges from $1.00 \times 10^4 - 4.39 \times 10^6 \text{ m}^2$ $(0.01 - 4.39 \text{ km}^2)$, with a mean area of $1.65 \times 10^5 \text{ m}^2$ (0.165 km^2).

2.3 Boundary conditions

We set the boundary condition for hydraulic head at the glacier terminus as a Dirichlet condition, based on the ideas that the terminus is grounded and that pressure at the subglacial outflow should be equal to hydrostatic pressure from the overlying fjord water (depth varying across the front). Setting the subglacial water pressure equal to the pressure in the fjord at the subglacial outflow gives

$$\rho_w g(h - z_b) = \rho_f g d, \tag{10}$$

where ρ_f is the density of the fjord water and d is the water depth ($d = -z_b$ is a positive quantity, where z_b is bed elevation relative to sea level, i.e. a negative quantity at the terminus). Rearranging, we solve for head:

$$h = \frac{\rho_f}{\rho_w}d + z_b = \left(\frac{\rho_f}{\rho_w} - 1\right)d, \tag{11}$$

where $\rho_f/\rho_w > 1$. If the water at the subglacial outflow is assumed to be well-mixed with fresh water from melting at the glacier front, then $\rho_w \approx \rho_f$, and therefore $h \approx 0$ at the outflow. In other recent simulations of Helheim subglacial hydrology, Stevens and others (2022) assumed a floating terminus.

We prescribe Neumann conditions on the upstream and lateral boundaries of the model domain, with $\nabla h = \mathbf{0}$ at these boundaries.

2.4 Experiment description

Using the reduced form of the SHAKTI model as described above, we conduct simulations to produce a representation of the minimal winter base-state hydrological system of Helheim Glacier. In winter, no surface meltwater is produced, and meltwater inputs that reach the bed from the surface are presumed to be essentially zero over most of the Greenland Ice Sheet. Accordingly, we assume the absence of discrete features (e.g. moulins) or delayed drainage from features such as firn aquifers, in contrast to Poinar and others (2017, 2019). This does not mean, however, that there is no water at the bed in winter, as water is generated at the glacier base (Eqn. (8)). To generate an estimate of the winter base state of the subglacial hydrological system of Helheim Glacier, we run a 'spin-up' SHAKTI simulation with zero meltwater input from the englacial system to the bed ($i_{e \to b} = 0$) with all water at the system produced by basal melt as calculated by Eqn. (8). The simulation is run for a period of 1 year, with a time step of 30 minutes.
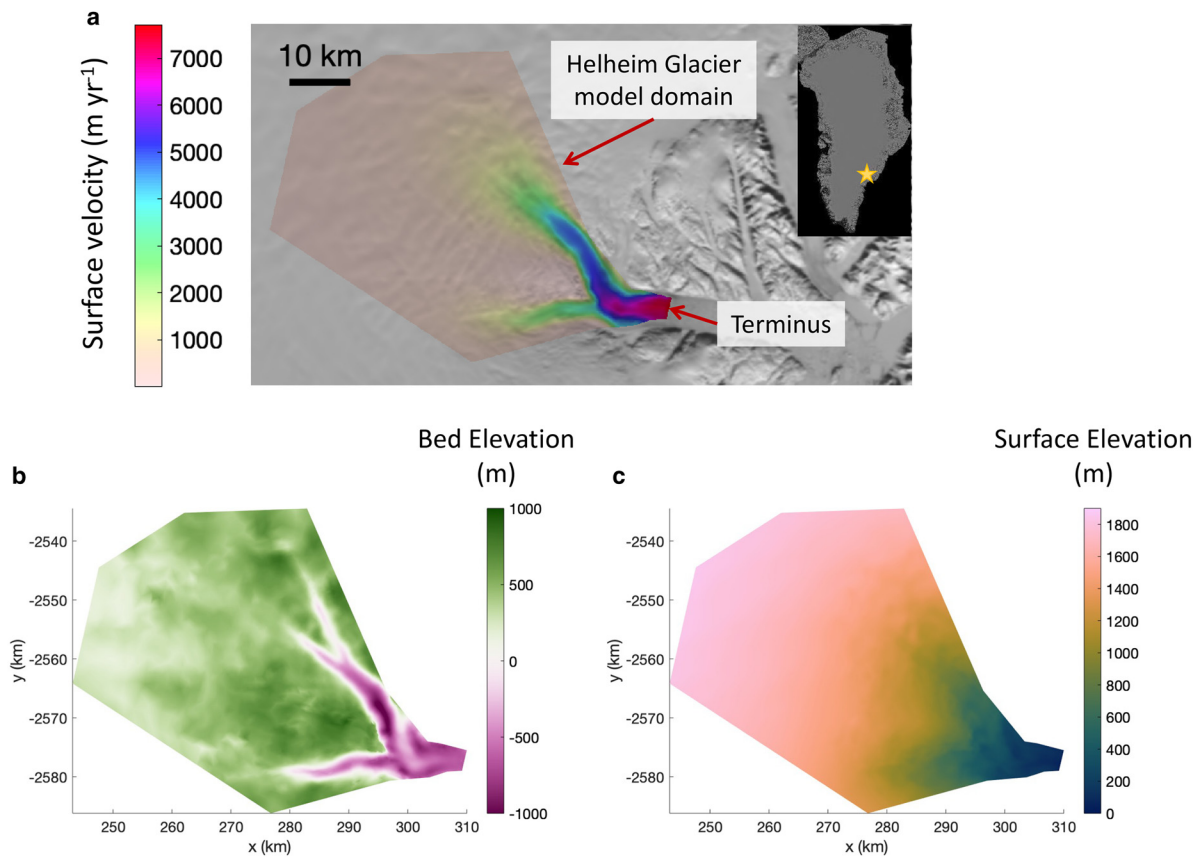
Figure 1. (a) Location of Helheim Glacier on the Greenland ice sheet (inset), velocity (Joughin and others, 2018) over model domain used in SHAKTI simulations, overlaid on 2010 MODIS mosaic (Haran and others, 2018), (b) bed topography in model domain relative to sea level (Morlighem and others, 2017, 2021), (c) surface elevation in model domain relative to sea level.

Figure S2 presents time series of various output quantities to demonstrate convergence of the system within this simulation duration.

In addition to this winter spin-up simulation, which we will refer to as *main*, we perform additional simulations using the same model domain, time step, and duration, to test and demonstrate the influence of frictional heat. We explore three different approaches of calculating the basal shear stress τ_b (involved in the frictional heating contribution to basal melt): 1) basal shear stress equal to the driving stress, $\tau_b = \rho_i g H |\nabla z_s|$, 2) basal shear stress equal to yield stress, depending on evolving effective pressure, $\tau_b = \mu N$, where μ is the till friction coefficient (Iverson, 2010), and 3) zero basal shear stress, $\tau_b = 0$, which effectively removes the influence of frictional heat from sliding.

Table 3 summarizes the simulations presented in this paper. The focus of this study is winter hydrology, and transient simulations will be the focus of a separate publication to maintain this focus. However, example simulation results with time-dependent forcing are shown in the supplementary material (Figs. S6 and S7) to illustrate the robustness of the reduced SHAKTI model with realistic topography under seasonal conditions.

Table 3. Summary of simulations

| Name	Description
main	Winter spin-up with $\tau_b = C^2 N |\mathbf{u}_b|$
drivingstress	Winter spin-up $\tau_b = \rho_i g H |\nabla z_s|$
yieldstress	Winter spin-up $\tau_b = \mu N$
nofrictionheat	Winter spin-up with no frictional heat, $\tau_b = 0$

3. Results

3.1 Winter base state

In Figure 2, we present the spatial distribution of the subglacial drainage system at the completion of the *main* simulation base-state spin-up. In this winter base state with zero external meltwater input, large portions of the bed exhibit high water pressure as demonstrated by a fraction of overburden, p_w/p_i, that is close to one (Fig. 2a). Distinct preferential drainage pathways emerge with larger gap height (Fig. 2b) and higher Reynolds number and water flux (Re, Fig. 2c) forming river-like structures. The major river-like structures coincide with the locations of deeply incised bedrock channels. Effective pressure is highly variable across the domain, lowest near the terminus and lower in the main drainage pathways than in the surrounding bed (Fig. 2d). Regions of turbulent flow ($Re > 10^3$) as well as regions of laminar flow ($Re < 10^3$) coexist (Fig. 2c), with clearly higher Re in the main pathways and in smaller arborescent tributaries that feed them. Most of the bed away from the main pathways has very low Re (i.e., very low flux, since $|q| = Re\ \nu$), with regions that appear to be poorly connected. A clear primary outflow structure emerges at the terminus, located slightly south of the center line. This preferential discharge location agrees well with the location of observed summertime subglacial plumes upwelling at Helheim (Everett and others, 2021; Melton and others, 2022) and with the consistent outflow point as simulated by Stevens and others (2022).

3.2 Spatially variable transmissivity

In recent years, the community has highlighted the importance of hydraulically isolated and weakly connected regions of the bed in
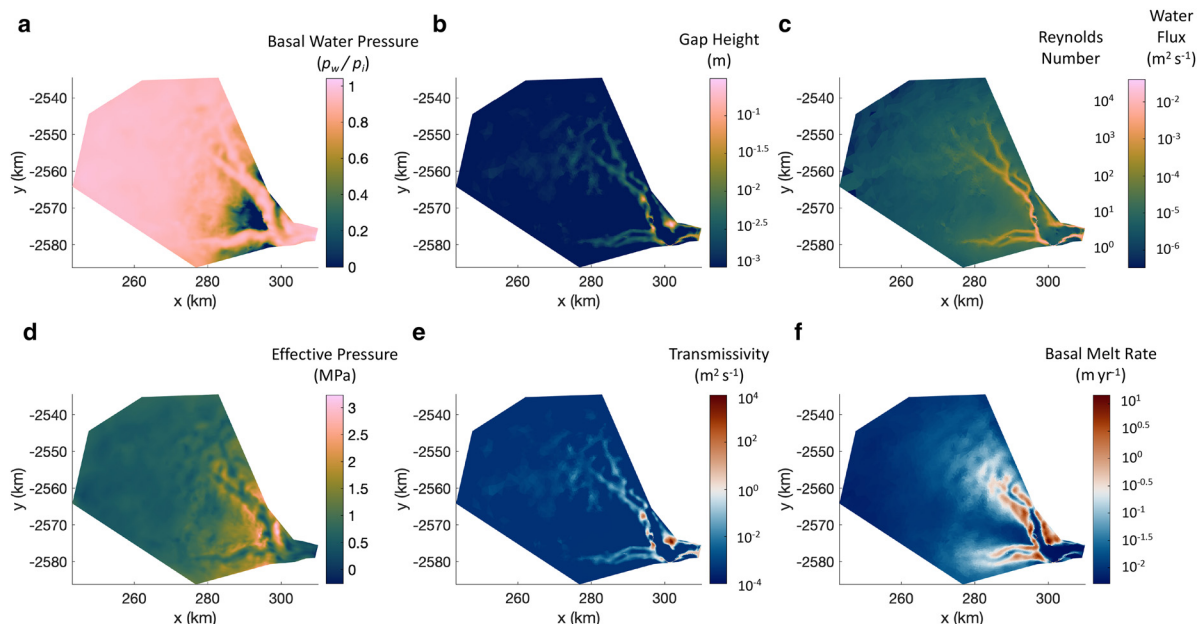
Figure 2. Winter base state of subglacial hydrological system with zero external meltwater input (*main* simulation): (a) water pressure as fraction of overburden, p_w/p_i, (b) gap height (shown in $\log_{10}$ scale for detail), (d) Reynolds number and basal water flux (shown in $\log_{10}$ scale for detail), (d) effective pressure, (e) transmissivity (shown in $\log_{10}$ scale for detail), (f) basal melt rate (shown in $\log_{10}$ scale for detail).

subglacial hydrology, particularly for maintaining observed high winter water pressures (Andrews and others, 2014; Hoffman and others, 2016; Rada and Schoof, 2018; Mejía and others, 2021; Rada Giacaman and Schoof, 2023). An advantage of SHAKTI is that the flux formulation (Equation (6)) incorporates spatially and temporally variable hydraulic transmissivity, rather than requiring a prescribed value for hydraulic conductivity as in other models. As shown in Figure 2e, we find highly heterogeneous transmissivity values, varying over several orders of magnitude within the Helheim domain. Simulated transmissivity is highest near the terminus and along the main winter drainage pathways, and is particularly low along the divide between the two main branches of fast ice flow, as well as through the center of each of these ice streams. The low-transmissivity regions in the center of the main ice flow branches coincide with topographical ridges in the bed, particularly in the northern branch. These low-transmissivity areas represent regions with little connectivity and water flow through them, or in other words are interpreted as poorly connected. In groundwater aquifers, transmissivity of $K < 5$ m^2 d^{-1} is considered to be negligible, $5 < K < 50$ m^2 d^{-1} is weak, $50 < K < 500$ m^2 d^{-1} is moderate, and $K > 500$ m^2 d^{-1} is high (De Wiest, 1965). Considering the weak transmissivity threshold of $K \leq 50$ m^2 d^{-1}, 71% of the bed by area in our model domain is interpreted to be poorly connected in the winter.

The full range of hydraulic transmissivity shown in Figure 2e spans a range of 4.3×10^{-4} to 5.9×10^3 m^2 s^{-1}. To put our simulated transmissivity values into context of some other subglacial hydrology studies, Stevens and others (2022) simulated partially overlapping range of transmissivity of 9.8×10^{-5} to 9.8 m^2 s^{-1} (based on reported transmissivity values for one point of $T = 1 \times 10^{-8}$ to 1×10^{-3} Pa^{-1} s-1 with transmissivity defined in terms of pressure gradient, converted to standard transmissivity units of m^2 s^{-1} as $T\rho_w\, g$ for comparison to our transmissivity dependent on hydraulic head gradient). Inferring transmissivity from GPS measurements in response to lake drainage events, assuming Darcy flow through porous media at the bed, Lai and others (2021) estimated transmissivity of 4.4×10^{-3} to 1.2 m^2 s^{-1} (based on reported kh_0 values of 0.8 to 215 mm^3, converted to units of m^2 s^{-1} as $kh_0 g/\nu$). In modeling a land-terminating region in west Greenland, Dow and others (2015) calculated

transmissivity of 2.5×10^{-3} to 0.2 m^2 s^{-1}, with a 'baseline' value of 1.5×10^{-2} m^2 s^{-1}, based on different values for sheet 'conductivity' (units of m s^{-1}) and critical sheet thickness (units of m).

Our simulated transmissivity spans a much wider range than what has been previously inferred. To examine the spatial distribution of transmissivity and relation to water pressure, Figure 3 presents transmissivity as a function of water pressure (as fraction of overburden), grouped by region designated by surface elevation. The broadest range of transmissivity emerges in the low-elevation region, with $z_s \leq 900$ m. The intermediate elevation class, between 900 and 1500 m surface elevation, inhabits a middle range of transmissivity, while the highest elevation region in the interior ($z_s \geq 1500$ m) is broadly characterized by high fraction of overburden and very low transmissivity.

3.3 Basal melt

Basal melting has increasingly been acknowledged as an important consideration for ice dynamics (Karlsson and others, 2021; Young and others, 2022). As described in Equation (8), basal
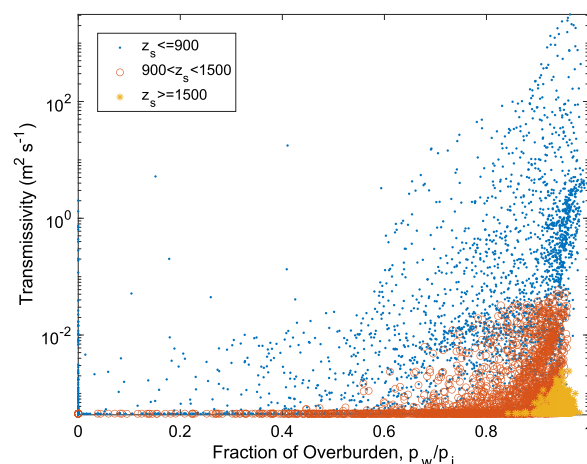
Figure 3. Winter hydraulic transmissivity (K) as a function of water pressure (as a fraction of overburden, p_w/p_i) for different regions of the model domain based on surface elevation.
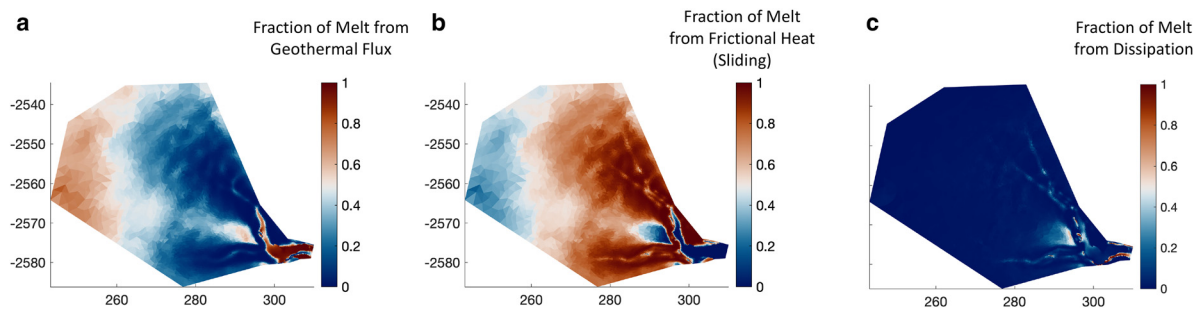
Figure 4. (a) Fraction of basal melt rate due to geothermal flux, (b) fraction of basal melt rate due to frictional heat from sliding, (c) fraction of basal melt rate due to dissipation.

meltwater is produced at the bed through geothermal flux, frictional heat from sliding of the ice over the bed, and turbulent dissipation, in which mechanical energy is converted to thermal energy in the water flow. The mean melt rate over the entire domain is 0.097 m yr^{-1} and the total melt rate over the domain is 6.3 m^3 s^{-1}. Previous work exploring subglacial hydrology at Helheim or on an idealized Helheim-like domain using other subglacial hydrology models invoke a prescribed uniform background basal melt rate to account for geothermal and frictional heat (Poinar and others, 2019; Stevens and others, 2022). In Figure 4, we present the fraction of basal melt rate due to geothermal flux (Fig. 4a), frictional heat (Fig. 4b), and dissipation (Fig. 4c). Geothermal flux is applied in our simulation with a uniform value of 0.05 W m^{-2}, but in reality this varies spatially and may vary by up to a factor of two in narrow incised canyons (Colgan and others, 2021; Willcocks and others, 2021). Frictional heat dominates over most of the domain, yielding the highest melt rates along the steep topographic walls of the deeply incised bed canyons. Dissipation is an important source of basal melt in the primary outflow to the terminus, even in winter.

In the results presented above, the basal stress $\tau_b = C^2 N |\mathbf{u}_b|$, where τ_b evolves transiently with N and basal velocities are held constant in time. The spatially variable drag coefficient, C, shown in Figure 5a, is obtained through inverse modeling using ISSM, assuming effective pressure $N = \rho_i g H + \rho_w g z_b$, the standard practice for basal drag inversion in ISSM (although the distribution of N obviously evolves in our SHAKTI simulations). The inversion optimizes C in order for the ice flow model to reproduce observed surface velocities through the ice stress balance. As we might expect intuitively, the resulting drag coefficient from inversion is high in areas of slow-moving ice (high friction) and low where the ice is sliding rapidly (high slip rates, i.e. in the main glacier branches and near the terminus). Basal shear stress at the end

of the *main* simulation (Fig. 5b) varies over many orders of magnitude, with the highest stress along the walls of the main branches and throughout the interior, with lowest stress near the terminus and particularly along the primary discharge pathway.

Now we consider the three winter simulations with different approaches to calculate the basal shear stress τ_b: 1) basal shear stress equal to the driving stress, $\tau_b = \rho_i g H |\nabla z_s|$ (*drivingstress*), 2) basal shear stress equal to yield stress, depending on evolving effective pressure, $\tau_b = 0.3N$, where 0.3 is the till friction coefficient (*yieldstress*), and 3) zero basal shear stress, $\tau_b = 0$, which effectively removes the influence of frictional heat from sliding (*nofrictionheat*).

The resulting winter base-state hydrological system differs substantially between these three cases and our original *main* winter simulation. Overall, effective pressure is higher over most of the domain (corresponding to lower water pressure) when frictional heat is included than for the case with $\tau_b = 0$ (Fig. 6a). *Drivingstress* and *yieldstress* produce higher basal stress than our *main* simulation (Fig. 6b), and correspondingly lead to higher melt rates. With basal shear stress equal to driving stress or yield stress, frictional heat from sliding is the vastly dominant source of basal melt rate over most of the domain and leads to much higher flux through the main branches of the glacier, blurring the distinct drainage pathways that emerge in our *main* simulation and in the *nofrictionheat* simulation, as illustrated by the distribution of basal water flux in each simulation (Fig. 7). In our *main* simulation, water flux and basal melt rates are high along the walls of the deeply incised bed troughs (Figs. 2f and 7a). Better defined flow paths are visible than in the *drivingstress* and *yieldstress* simulations, but the drainage regime is distinctly more developed with a higher flux of water compared to the *nofrictionheat* case.
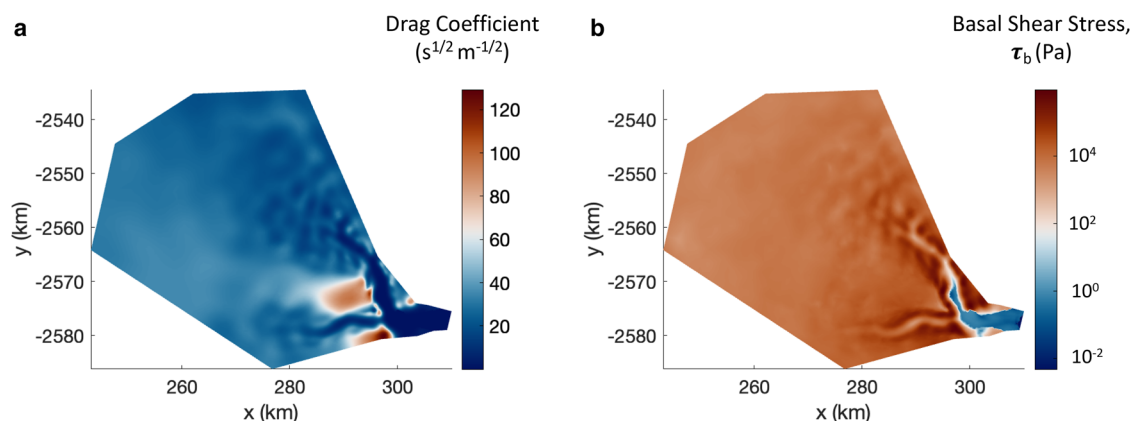
Figure 5. (a) Drag coefficient used in *main* simulation basal stress calculation, (b) winter basal shear stress, $\tau_b = C^2 N |\mathbf{u}_b|$.
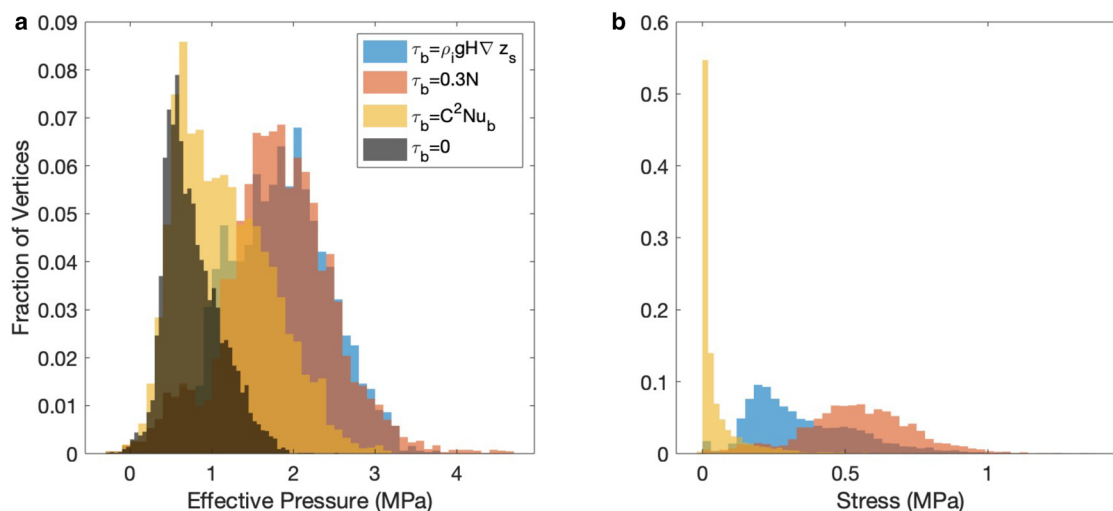
Figure 6. Histograms comparing different approaches for basal shear stress τ_b: (a) resulting effective pressure distribution, (b) basal shear stress.

We find that total basal melt rates and subglacial discharge at the terminus vary substantially depending on the frictional heat calculation. The total basal melt rate and outflow at the terminus with *frictionheat* are lower than in our *main* simulation, and several times higher with *yieldstress* and *drivingstress*, as summarized in Table 4.

4. Discussion

4.1 High water pressure in winter

While models have achieved good qualitative behavior for melt-season evolution (Hewitt, 2013; Werder and others, 2013), a challenge of subglacial hydrology modeling has been to reproduce high water pressures in winter conditions to agree with borehole measurements (Flowers, 2015). Note that most borehole measurements of high winter water pressure have been taken in land-terminating portions of west Greenland, with no borehole measurements to the bed at Helheim Glacier. Disconnected, weakly connected, or isolated regions of the bed have been shown to be necessary for maintaining high winter water pressure in other subglacial hydrology models (Hoffman and others, 2016; Rada and Schoof, 2018). Our winter SHAKTI simulation of Helheim successfully produces widespread high water pressure (Figs. 2a, S3) that corresponds with low transmissivity in the interior (Fig. 2e), suggesting that the transitional flux formulation of SHAKTI (Equation (5)) enables representation of winter high-pressure regions with a continuum approach.

Recently, Stevens and others (2022) simulated subglacial hydrology at Helheim with a different model (Hewitt, 2013; Stevens and others, 2018). While their winter simulation produced high water pressure (low effective pressure) in the main
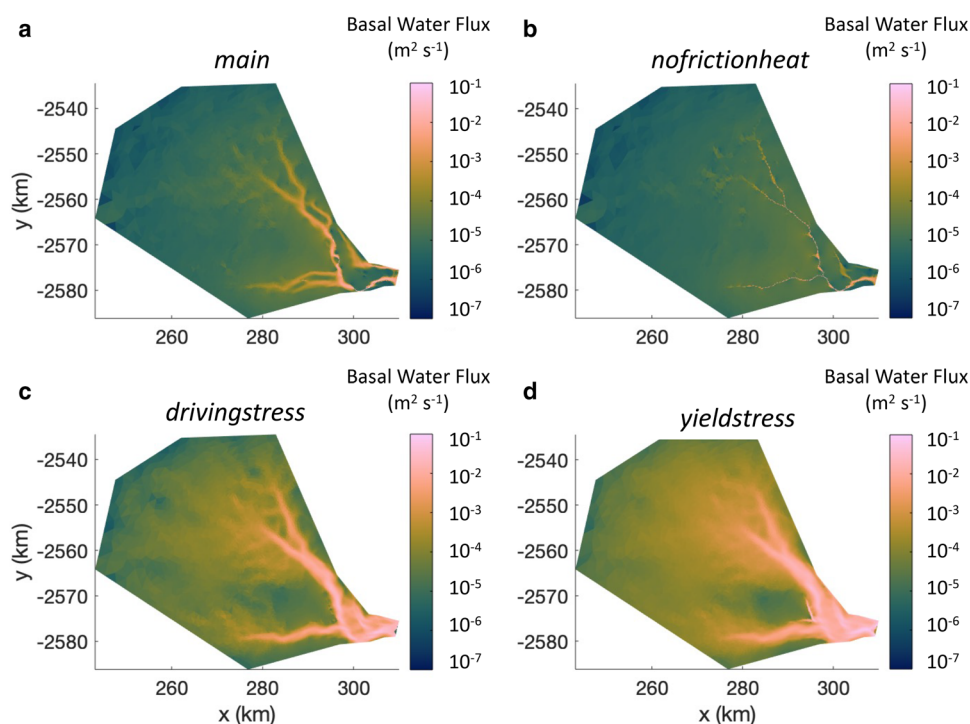
Figure 7. Winter basal water flux (shown in $\log_{10}$ scale for detail) resulting from different approaches for basal shear stress τ_b: (a) drag coefficient from ISSM inversion, (b) no frictional heat, (c) driving stress, (d) yield stress.

Table 4. Subglacial discharge at terminus and total basal melt rate over model domain

Simulation	Discharge at terminus	Total basal melt rate
main	10.2 m^3 s^{-1}	6.3 m^3 s^{-1}
drivingstress	75.8 m^3 s^{-1}	65.2 m^3 s^{-1}
yieldstress	130.8 m^3 s^{-1}	112.0 m^3 s^{-1}
nofrictionheat	2.7 m^3 s^{-1}	0.4 m^3 s^{-1}

trunk of the glacier near the terminus, the interior portions of their domain extending up the two main branches were simulated to exist at effective pressure of $N = 6$ MPa or more during the winter, which is significantly higher than the maximum effective pressure of $N = 3.2$ MPa in our *main* simulation. Key differences in our approach compared to Stevens and others (2022) that likely play a role in this difference are the transitional flux (Equation (5)) used in SHAKTI, and spatially variable basal stress.

4.2 Role of basal topography

The predictions for winter subglacial water pressure in Figures 2a and S3 show variability across a range of length scales. Hydropotential flow routing (Shreve, 1972) is commonly used to predict possible subglacial paths. This is typically done by assuming the water pressure to be equal to overburden everywhere ($p_w/p_i =$ 1.0), or some other uniform fraction of overburden. However, as shown in Figure 2a, we find that the fraction of overburden varies considerably, spanning the entire range from 0 to 1 over the whole domain, and spanning from $\sim 0.7 - 1$ in regions of faster ice flow. Assuming a uniform fraction of overburden may thus yield an inaccurate picture of subglacial drainage (Wright and others, 2008). In Figure 8, we compare the difference in head distributions from a uniform fraction of overburden and our winter SHAKTI simulation. An assumption of water pressure equal to 100% overburden pressure ($p_w = p_i$, i.e. a uniform fraction of overburden $p_w/p_i = 1.0$) overpredicts head in the vast majority of the domain, except very near the terminus where it agrees with the results of our SHAKTI simulation (Fig. 8a). Assuming water pressure equal to 80% overburden pressure ($p_w = 0.8p_i$, i.e. a uniform fraction of overburden $p_w/p_i = 0.8$) agrees better, but still overestimates head in the more stagnant portions of the domain lateral to the main drainage pathways and underestimates head near the terminus, in the river-like features themselves, and further inland regions (Fig. 8b). Any other assumed uniform fraction of overburden will similarly not account for spatial variations in pressure distribution.

In the presence of steep topographic gradients, as encountered beneath Helheim Glacier, the deeply incised bed topography (and its reflection in surface topography) largely determines the locations of the main drainage paths. Recall that flow is driven by the hydraulic head gradient, and hydraulic head is composed of two components, pressure head and elevation head: $h = p_w/(\rho_w g) + z_b$. In the case of localized canyons with bed elevation well below sea level, the elevation head in these troughs is sufficiently low to attract water from the surrounding areas, even when the water pressure is higher at the bottom of the canyons. As shown in Figure 8c, similar primary drainage pathways through the deep bed canyons emerge when using a simple routing calculation assuming water pressure equal to 100% overburden everywhere (compare to *Re* distribution in Fig. 2d). This is true using other uniform fractions of overburden as well, but the configuration of tributary drainage feeding the deep canyons differs, along with the resulting pressure distribution as shown in Figures 8a,b.

For purposes of identifying primary drainage paths, hydropotential routing provides a good estimate, assuming accurate bed topography, particularly in places with high-relief mountainous features. To investigate processes involving broad areas of the bed and drainage tributaries, however, spatially heterogeneous pressure distribution must be considered.

4.3 Winter priming of the drainage system

Our winter base-state *main* simulation highlights the fact that there is widespread subglacial drainage present year-round under Helheim Glacier, with at least a minimal system supported by basal meltwater generated by geothermal flux, frictional heat from sliding, and dissipated heat from the water flow, as considered here. At Sermeq Kujalleq (Store Glacier), a tidewater glacier in west Greenland, Cook and others (2020) also simulated an active winter subglacial drainage system, bolstered by winter discharge observations (Chauché and others, 2014). Our model results suggest that the drainage system at Helheim does not begin from a totally shut-down state at the initiation of melt each year, but retains some form through the winter. The 'deflated' drainage structure without surface meltwater input includes preferential pathways and large areas of low-transmissivity bed, primed to spring into more efficient drainage action with the delivery of surface-generated meltwater to the bed. With our winter simulation results in mind, the seasonal evolution of drainage efficiency and structure may not depend only on the spatio-temporal distribution of moulins and crevasses for meltwater inputs from the surface to the bed (or from englacial drainage of firn aquifers or other storage voids), but is likely also a function of the persistent winter base-state drainage structure. Therefore, we recommend considering an existing winter drainage system when interpreting observational data.

Previous work has explored the idea of winter priming beneath the Greenland Ice Sheet. In west Greenland, Chu and others (2016) found water stored on bed ridges in winter, which then
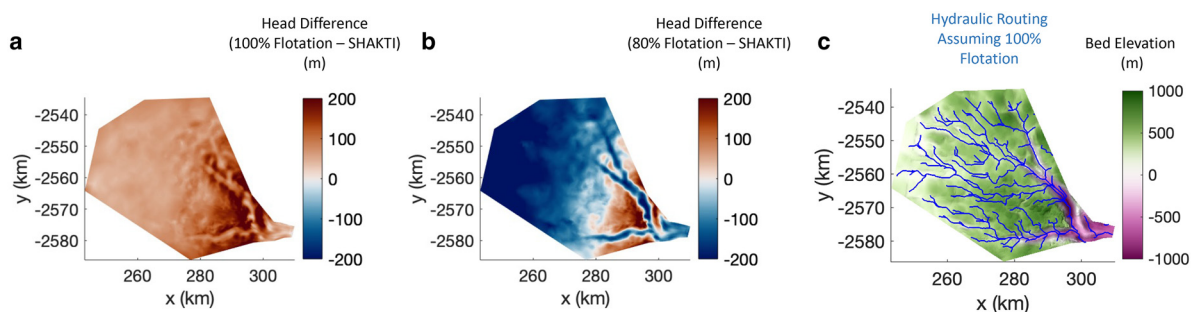
Figure 8. (a) Difference in hydraulic head between water pressure assumed equal to 100% overburden pressure ($p_w/p_i = 1.0$) and that calculated in our *main* winter SHAKTI simulation. (b) Difference in hydraulic head between water pressure assumed equal to 80% overburden pressure ($p_w/p_i = 0.8$) and our *main* simulation. (c) Streamlines based on hydraulic potential flow routing with assumed 100% overburden pressure.

flows to depressions and troughs in the melt season. Poinar and others (2019) simulated subglacial hydrology of an idealized Helheim-like glacier (without realistic bed topography) with year-round drainage of firn aquifer water to the bed, finding that increased water at the bed during winter facilitated more rapid and pronounced development of efficient channel networks in the melt season. The winter base state documented here would play a key role in that priming action, and shows that wintertime firn aquifer drainage may not be necessary in order to have year-round channelized structure at Helheim. This is largely because of the deeply incised canyons in the bed that preferentially pull water into river-like features even in the absence of meltwater inputs from the surface or englacial system, and this active winter channelized structure would likely be further enhanced by delayed meltwater drainage from the firn aquifer (Poinar and others, 2017). Recent work modeling Helheim subglacial hydrology by Stevens and others (2022) also simulated active drainage in the near-terminus region of Helheim under winter conditions.

4.4 River-like winter features

SHAKTI employs a continuum description of subglacial geometry, without distinguishing between different drainage-system components. The way SHAKTI represents the geometry is through the subglacial gap height b, which is an average of the gap height over an entire element (i.e. generalizing earlier work on spatially lumped models such as Schoof, 2010; Brinkerhoff and others, 2016). This means that SHAKTI does not resolve individual drainage channel geometry by calculating semi-circular cross-sectional area as in some other models (Hewitt, 2013; Werder and others, 2013; Meyer and others, 2016, 2017; Felden and others, 2023). The primary variable sought from subglacial hydrology models for ice dynamics calculations is the subglacial water pressure (or equivalently, effective pressure), which influences sliding velocity. The subglacial water pressure field is relatively smooth compared to small-scale geometric variations (e.g. in gap height at the bed) within a subglacial system. Without distinguishing different drainage modes with different evolution equations in each, SHAKTI is able to represent both distributed and channelized sub-systems naturally. With realistic bed topography incorporated, the winter simulation results presented above suggest the promise of SHAKTI in representing weakly connected sub-systems as well. The winter features reminiscent of broad channels have higher water pressure than their surroundings in this winter base state, but lower head, which is what drives the flux of water from the surrounding areas into these pathways due to the deeply incised bed. These river-like features will likely transition with seasonal meltwater input into even more efficient drainage channels. Stevens and others (2022) also simulated substantial subglacial flow at Helheim with high-pressure channels persisting within 10 km of the terminus, even in winter, although that study considered a model domain focused on the near-terminus region without extending as far inland but employing a prescribed incoming flux from their upstream boundaries.

Note that the primary drainage pathways exist close to overburden pressure in winter. Recent work by Dow and others (2022) simulated large, high-pressure channels extending far inland in Antarctica at close to overburden pressure, although their simulation results were sensitive to prescribed channel and sheet conductivities required by the GlaDS model. The existence of large, high-pressure channelized structures under thick ice is a relatively new idea, diverging from than the classical theory of low-pressure R-channels (Röthlisberger, 1972). In some ways, interior regions of Greenland in the winter with no surface melt are similar to Antarctica. If Antarctica begins to experience more surface melt farther inland, this raises the possibility that it could potentially transition to become similar to Greenland in terms of seasonal hydrology behavior.

4.5 Role of basal stress in calculating frictional heat

Basal melt from frictional heat generated by sliding of the ice over its bed is potentially a dominant source of basal melt, as shown in Figure 4 and according to basal melt rates for Greenland calculated by Karlsson and others (2021), especially in fast-flowing glaciers like Helheim (which moves rapidly even in winter, with winter velocities exceeding 8,000 m yr^{-1}) (Kehrl and others, 2017). The total basal melt rate we find for Helheim in the *main* simulation (6.3 m^3 s^{-1}, Table 4) is similar to the melt rate of 5.96 m^3 s^{-1} calculated for Store Glacier in west Greenland by Cook and others (2020). This estimate was produced with a different model formulation and for a smaller, slower-flowing glacier than Helheim, but provides some corroboration for the theory that using driving stress or yield stress as proxies for basal stress may over-predict basal melt rates.

High localized basal melt rates on the order of 20 m yr^{-1} are calculated in our *drivingstress* and *yieldstress* simulations (Fig. S4), two orders of magnitude higher than the maximum melt rate in the *nofrictionheat* simulation without frictional heat from sliding, 1.0 m yr^{-1}. In our original simulation with $\tau_b = C^2 N u_b$, the maximum local melt rate is 14.4 m yr^{-1} (Fig. 2f). The plausibility of such high wintertime local melt rates is unresolved, as this rate of basal melt is inconsistent with most observations to date. Young and others (2022) inferred basal melt rates of this order of magnitude in west Greenland, but in the context of a summer rain event, not a winter background melt rate. Greenland basal melt rates as calculated by Karlsson and others (2021) are typically < 0.25 m yr^{-1}, which agrees better with our *nofrictionheat* simulation. In previous work on a Helheim-like idealized glacier, Poinar and others (2019) prescribed a uniform basal melt rate of 0.02 m yr^{-1} (based on thermomechanical modeling by Aschwanden and others, 2012). In modeling subglacial hydrology at Helheim, Stevens and others (2022) also prescribed a uniform basal melt rate of 0.0262 m yr^{-1} to represent geothermal and frictional heat contributions. The high melt rates in our simulations are extremely local; the average basal melt rate over a larger area is lower (mean of 0.097 m yr^{-1} over the entire model domain in our *main* simulation). With high localized basal melt rates included in an ice-dynamics model like ISSM, unusual features may result or the ice would need to compensate by flowing in to fill these melting 'sinks'. This is an interesting topic to pursue in coupled simulations of hydrology and thermo-mechanical ice dynamics.

Given the disparity between the *nofrictionheat* simulation and the simulations using various formulations for basal shear stress, we demonstrate that frictional heat is an influential control on determining subglacial drainage regimes. This is not entirely satisfying from a modeling perspective. To add to the complexity, friction at the ice-bed interface may not be as straightforward as is frequently assumed, and heat may be generated deeper in the basal sediment as discussed by Hansen and Zoet (2022), which we do not include in our simulations. We must carefully consider what is likely to be a realistic drainage configuration at Helheim Glacier in the winter. Should we expect widespread high water pressure and clearly defined river-like pathways strongly influenced by the bed topography as we find in our *main* simulation? Or could there be sufficient heat generated by rapid sliding over the bed so that the water flow is actually more distributed and widespread through the main branches of the glacier without as distinct river-like features, as seen by using driving stress or yield stress for basal shear stress? Including frictional heat from

sliding with these latter two methods leads to higher effective pressure (lower water pressure) over most of the interior domain (Figs. 6a and S5), contrary to our modeling target of reproducing high water pressure in winter. We are encouraged by the success of our *main* simulation that invokes drag coefficient and friction based on ISSM inversion in producing widespread winter water pressures and poorly connected regions of the bed.

Recent work by Stevens and others (2022) to simulate subglacial hydrology at Helheim used a spatially uniform and temporally constant formulation to represent frictional heat over their domain, based on a value of basal shear stress of 60 kPa and a sliding velocity of 500 m yr^{-1}. This approach does not capture the spatial variation in the contribution from frictional heat to basal melt, considering that much of the near-terminus region of Helheim has a persistent velocity of several km per year. We calculate basal stress lower than 60 kPa near the terminus and an order of magnitude higher (10^5 Pa) along the walls of the deep bed canyons (Fig. 5b).

Interestingly, the amount of meltwater produced in the domain is significantly greater when using driving stress as basal stress (*drivingstress* simulation) compared to the *main* simulation (Table 4). Over large scales, the basal shear stress should average to the driving stress, so these results imply that basal shear stress is concentrated in slower-flowing regions and along edges of fast-sliding areas (as seen in τ_b from *main*, Fig. 5b). Employing driving stress as a proxy for basal stress in fast-flowing regions like the main branches of Helheim leads to an overprediction of frictional heat. Admittedly, in simulations coupling effective pressure and ice velocity, the basal stress should match the driving stress well over large areas as the velocity adjusts to evolving effective pressure. In our stand-alone SHAKTI simulations assuming steady velocity, basal drag in the interior drifts from driving stress. This serves as excellent motivation for further work coupling hydrology and velocity. Future work employing a fully coupled model will provide improved insights on integrated mass-momentum-energy balances at the ice-water interface.

4.6 Seasonal meltwater inputs

To illustrate the capacity of the reduced SHAKTI model to handle transient meltwater inputs and the recovery period to winter conditions for interested readers, we also include results from a sample transient simulation with a duration of one year in the supplementary material (Figs. S6 and S7), applying distributed meltwater input (term $i_{e \to b}$ in Equation (2)). The magnitude of meltwater applied to the bed is based on 2020 MERRA-2 data for a location in the main trunk of Helheim (GMAO, 2015), with hourly meltwater inputs smoothed over a period of 14 days. Beginning from the winter base state obtained through our *main* simulation, we supply seasonal meltwater inputs to the system at low elevations (surface elevation ≤900 m) to simulate the full annual 2020 cycle. Given that lower Helheim contains substantial crevassed regions, surface meltwater input does not necessarily reach the bed through point inputs such as moulins, as in western Greenland, and we have elected to approximate these low-elevation inputs as distributed evenly over the bed to represent widespread crevassing.

To maintain the focus of this work on winter base-state hydrology and the reduced SHAKTI model formulation, this simple transient simulation does not consider delayed drainage from the firn aquifer at higher elevations as in Poinar and others (2019) or lake drainages as in Stevens and others (2022), but is included purely as an uncomplicated demonstration of the robustness of the reduced SHAKTI model to handle transient meltwater inputs and produce results within realistic ranges.

5. Conclusions

In this paper, we describe a reduced form of the SHAKTI subglacial hydrology model, retaining only the essential dynamics and parameterizations that do not involve poorly constrained parameters. We demonstrate the utility of SHAKTI by simulating the winter base-state drainage of Helheim Glacier in east Greenland. Like all models, SHAKTI is an approximation to a complex natural system, paving the way for large-scale coupled simulations. Stand-alone hydrology models such as SHAKTI are useful for understanding evolution of subglacial pressure and flow, but must be coupled to ice dynamics models to fully capture the reciprocal influences of effective pressure and glacier sliding. This coupling is an active area of ongoing work, and is beyond the scope of the present paper.

With the reduced SHAKTI model, we are able to: (a) reproduce widespread areas of high water pressure in winter using a continuum model, which are widely documented in field measurements and have been difficult to reproduce with subglacial hydrology models, and (b) demonstrate that hydraulic transmissivity, as calculated with the transitional flux formulation of SHAKTI, varies over several orders of magnitude within the domain, naturally representing poorly connected regions of the bed with a continuum approach.

Water pressure as a fraction of overburden varies substantially across the domain. While the locations of the main drainage pathways at Helheim are driven by the deeply incised topographic features in the bed and their corresponding effect in the ice surface slope, spatial pressure variations influence the overall flow configuration.

Frictional heat from sliding is the dominant source of basal melt rate over much of the domain, particularly in the interior, yielding high melt rates especially along the steep walls of bed incisions. The method used to calculate basal stress has a large influence on overall melt rate and the resulting drainage configuration and basal water flux. We find that using driving stress or yield stress as a proxy for basal stress both over-predict basal melt in fast-flowing areas compared to an approach that involves drag coefficients derived from inverse ice dynamics modeling. In summary, frictional heat from sliding is influential in the context of fast-flowing glaciers, and should be carefully considered in modeling subglacial hydrology and ice dynamics.

Finally, an important question for further research is to clarify the relationship between bed topography, basal melt rates, and maintenance of the subglacial hydrologic system.

References

Andrews LC and 7 others (2014) Direct observations of evolving subglacial drainage beneath the Greenland Ice Sheet. *Nature* **514**(7520), 80–83. doi: 10.1038/nature13796

Aschwanden A, Bueler E, Khroulev C and Blatter H (2012) An enthalpy formulation for glaciers and ice sheets. *Journal of Glaciology* **58**(209), 441–457. doi: 10.3189/2012JoG11J088

Banwell A, Hewitt I, Willis I and Arnold N (2016) Moulin density controls drainage development beneath the Greenland Ice Sheet. *Journal of*

Geophysical Research: Earth Surface **121**(12), 2248–2269. doi: [10.1002/2015JF003801](10.1002/2015JF003801)

Brinkerhoff DJ, Meyer CR, Bueler E, Truffer M and Bartholomaus TC (2016) Inversion of a glacier hydrology model. *Annals of Glaciology* **57**, 1–12. doi: [10.1017/aog.2016.3](10.1017/aog.2016.3)

Budd W, Keage P and Blundy N (1979) Empirical studies of ice sliding. *Journal of Glaciology* **23**(89), 157–170. doi: [10.3189/S0022143000029804](10.3189/S0022143000029804)

Chauché N and 8 others (2014) Ice–ocean interaction and calving front morphology at two west Greenland tidewater outlet glaciers. *The Cryosphere* **8**(4), 1457–1468. doi: [10.5194/tc-8-1457-2014](10.5194/tc-8-1457-2014)

Chaudhuri A, Rajaram H and Viswanathan H (2013) Early-stage hypogene karstification in a mountain hydrologic system: A coupled thermohydro-chemical model incorporating buoyant convection. *Water Resources Research* **49**(9), 5880–5899. doi: 10.1002/wrcr.20427

Chu W and 5 others (2016) Extensive winter subglacial water storage beneath the Greenland Ice Sheet. *Geophysical Research Letters* **43**(24), 12–484. doi: [10.1002/2016GL071538](10.1002/2016GL071538)

Colgan W and 8 others (2021) Topographic correction of geothermal heat flux in Greenland and Antarctica. *Journal of Geophysical Research: Earth Surface* **126**(2), e2020JF005598. doi:[10.1029/2020JF005598](10.1029/2020JF005598).

Cook SJ, Christoffersen P and Todd J (2022) A fully-coupled 3D model of a large Greenlandic outlet glacier with evolving subglacial hydrology, frontal plume melting and calving. *Journal of Glaciology* **68**(269), 486–502. doi: [10.1017/jog.2021.109](10.1017/jog.2021.109)

Cook SJ, Christoffersen P, Todd J, Slater D and Chauché N (2020) Coupled modelling of subglacial hydrology and calving-front melting at Store Glacier, West Greenland. *The Cryosphere* **14**(3), 905–924. doi:[10.5194/tc-14-905-2020](10.5194/tc-14-905-2020)

Cowton T and 7 others (2013) Evolution of drainage system morphology at a land-terminating Greenlandic outlet glacier. *Journal of Geophysical Research: Earth Surface* **118**(1), 29–41. doi: [10.1029/2012JF002540](10.1029/2012JF002540)

Crameri F (2021) Scientific colour maps (7.0.1). *Zenodo*doi: 10.5281/zenodo.5501399

Creyts TT and Clarke GK (2010) Hydraulics of subglacial supercooling: theory and simulations for clear water flows. *Journal of Geophysical Research: Earth Surface* **115**(F3). doi: [10.1029/2009JF001417](10.1029/2009JF001417)

de Fleurian B and 9 others (2018) SHMIP the subglacial hydrology model intercomparison project. *Journal of Glaciology* **64**(248), 897–916. doi: [10.1017/jog.2018.78](10.1017/jog.2018.78)

De Wiest RJ (1965) *Geohydrology*. New York: John Wiley and Sons.

Dow CF and 9 others (2015) Modeling of subglacial hydrological development following rapid supraglacial lake drainage. *Journal of Geophysical Research: Earth Surface* **120**(6), 1127–1147. doi: [10.1002/2014JF003333](10.1002/2014JF003333)

Dow C, Ross N, Jeofry H, Siu K and Siegert M (2022) Antarctic basal environment shaped by high-pressure flow through a subglacial river system. *Nature Geoscience* **15**, 892–898. doi: [10.1038/s41561-022-01059-1](10.1038/s41561-022-01059-1)

Ehrenfeucht S, Morlighem M, Rignot E, Dow CF and Mouginot J (2023) Seasonal acceleration of Petermann glacier, Greenland, from changes in subglacial hydrology. *Geophysical Research Letters* **50**(1). e2022GL098009. doi: [10.1029/2022GL098009](10.1029/2022GL098009)

Everett A, Murray T, Selmes N, Holland D and Reeve DE (2021) The impacts of a subglacial discharge plume on calving, submarine melting, and mélange mass loss at Helheim Glacier, south east Greenland. *Journal of Geophysical Research: Earth Surface* **126**(3). e2020JF005910. doi:[10.1029/2020JF005910](10.1029/2020JF005910)

Felden AM, Martin DF and Ng EG (2023) SUHMO: an AMR SUbglacial Hydrology MOdel v1. 0. *Geoscientific Model Development* **16**16407–16425. doi:[10.5194/gmd-16-407-2023](10.5194/gmd-16-407-2023)

Flowers GE (2015) Modelling water flow under glaciers and ice sheets. *Proceedings of the Royal Society A: Mathematical, Physical and Engineering Sciences* **471**(2176). doi: 10.1098/rspa.2014.0907

Fudge T, Humphrey NF, Harper JT and Pfeffer WT (2008) Diurnal fluctuations in borehole water levels: configuration of the drainage system beneath Bench Glacier, Alaska, USA. *Journal of Glaciology* **54**(185), 297–306. doi: [10.3189/002214308784886072](10.3189/002214308784886072)

Gagliardini O and 9 others (2013) Capabilities and performance of Elmer/Ice, a new-generation ice sheet model. *Geoscientific Model Development* **6**(4), 1299–1318. doi: [10.5194/gmd-6-1299-2013](10.5194/gmd-6-1299-2013)

Gagliardini O and Werder MA (2018) Influence of increasing surface melt over decadal timescales on land-terminating Greenland-type outlet glaciers. *Journal of Glaciology* **64**(247), 700–710. doi: [10.1017/jog.2018.59](10.1017/jog.2018.59)

GMAO (2015) MERRA-2 tavg1_2d_lnd_nx v5.12.4, 2d,1-hourly,time-averaged, single-level,assimilation, land surface diagnostics v5.12.4, Greenbelt, MD, USA, Goddard Earth Sciences Data and Information Services Center (GES DISC), Accessed: January 6, 2022. doi: 10.5067/RKPHT8KC1Y1T.

Greene CA, Gwyther DE and Blankenship DD (2017) Antarctic mapping tools for MATLAB. *Computers & Geosciences* **104**, 151–157. doi: 10.1016/j.cageo.2016.08.003

Hansen D and Zoet L (2022) Characterizing sediment flux of deforming glacier beds. *Journal of Geophysical Research: Earth Surface* **127**(4). e2021JF006544. doi: [10.1029/2021JF006544](10.1029/2021JF006544)

Haran T, Bohlander J, Scambos T, Painter T and Fahnestock M (2018) MEaSUREs MODIS Mosaic of Greenland (MOG) 2005, 2010, and 2015 Image Maps, version 2. *NASA National Snow and Ice Data Center Distributed Active Archive Center, Boulder, Colorado USA*, 1162–1176 (doi: 10.5067/9ZO79PHOTYE5).

Harper JT, Humphrey NF, Pfeffer WT, Fudge T and O'Neel S (2005) Evolution of subglacial water pressure along a glacier's length. *Annals of Glaciology* **40**, 31–36. doi: [10.3189/172756405781813573](10.3189/172756405781813573)

Hewitt IJ (2011) Modelling distributed and channelized subglacial drainage: the spacing of channels. *Journal of Glaciology* **57**(202), 302–314. doi: [10.3189/002214311796405951](10.3189/002214311796405951)

Hewitt I (2013) Seasonal changes in ice sheet motion due to melt water lubrication. *Earth and Planetary Science Letters* **371**, 16–25. doi: 10.1016/j.epsl.2013.04.022

Hoffman MJ and 9 others (2016) Greenland subglacial drainage evolution regulated by weakly connected regions of the bed. *Nature Communications* **7**, 13903. doi: 10.1038/ncomms13903

Huss M, Bauder A, Werder M, Funk M and Hock R (2007) Glacier-dammed lake outburst events of Gornersee, Switzerland. *Journal of Glaciology* **53**(181), 189–200. doi: [10.3189/172756507782202784](10.3189/172756507782202784)

Iken A, Echelmeyer K, Harrison W and Funk M (1993) Mechanisms of fast flow in Jakobshavns Isbræ, West Greenland: Part I. Measurements of temperature and water level in deep boreholes. *Journal of Glaciology* **39**(131), 15–25. doi: [10.3189/S0022143000015689](10.3189/S0022143000015689)

Iverson NR (2010) Shear resistance and continuity of subglacial till: hydrology rules. *Journal of Glaciology* **56**(200), 1104–1114. doi: [10.3189/002214311796406220](10.3189/002214311796406220)

Jordan TM and 8 others (2018) A constraint upon the basal water distribution and thermal state of the Greenland Ice Sheet from radar bed echoes. *The Cryosphere* **12**(9), 2831–2854. doi: [10.5194/tc-12-2831-2018](10.5194/tc-12-2831-2018)

Joughin I, Smith BE and Howat IM (2018) A complete map of Greenland ice velocity derived from satellite data collected over 20 years. *Journal of Glaciology* **64**(243), 1–11. doi: [10.1017/jog.2017.73](10.1017/jog.2017.73)

Kamb B (1987) Glacier surge mechanism based on linked cavity configuration of the basal water conduit system. *Journal of Geophysical Research: Solid Earth* **92**(B9), 9083–9100. doi: [10.1029/JB092iB09p09083](10.1029/JB092iB09p09083)

Karlsson NB and 9 others (2021) A first constraint on basal melt-water production of the Greenland ice sheet. *Nature Communications* **12**(1), 1–10. doi: [10.1038/s41467-021-23739-z](10.1038/s41467-021-23739-z)

Kehrl LM, Joughin I, Shean DE, Floricioiu D and Krieger L (2017) Seasonal and interannual variabilities in terminus position, glacier velocity, and surface elevation at Helheim and Kangerlussuaq Glaciers from 2008 to 2016. *Journal of Geophysical Research: Earth Surface* **122**(9), 1635–1652. doi: [10.1002/2016JF004133](10.1002/2016JF004133)

Lai CY and 6 others (2021) Hydraulic transmissivity inferred from ice-sheet relaxation following Greenland supraglacial lake drainages. *Nature Communications* **12**(1), 3955. doi: [10.1038/s41467-021-24186-6](10.1038/s41467-021-24186-6)

Larour E, Seroussi H, Morlighem M and Rignot E (2012) Continental scale, high order, high spatial resolution, ice sheet modeling using the ice sheet system model (issm). *Journal of Geophysical Research: Earth Surface* **117**(F1). doi: [10.1029/2011JF002140](10.1029/2011JF002140)

Martos YM and 5 others (2018) Geothermal heat flux reveals the Iceland hotspot track underneath Greenland. *Geophysical Research Letters* **45**(16), 8214–8222. doi: [10.1029/2011JF002140](10.1029/2011JF002140)

Mejía J and 6 others (2021) Isolated cavities dominate Greenland Ice Sheet dynamic response to lake drainage. *Geophysical Research Letters* **48**(19), e2021GL094762. doi: [10.1029/2021GL094762](10.1029/2021GL094762)

Melton SM and 7 others (2022) Meltwater drainage and iceberg calving observed in high-spatiotemporal resolution at Helheim Glacier, Greenland. *Journal of Glaciology* **270**, 1–17. doi: [10.1017/jog.2021.141](10.1017/jog.2021.141)

Meyer CR, Fernandes MC, Creyts TT and Rice JR (2016) Effects of ice deformation on Röthlisberger channels and implications for transitions in subglacial hydrology. *Journal of Glaciology* **62**(234), 750–762. doi: [10.1017/jog.2016.65](10.1017/jog.2016.65)

Meyer CR, Hutchinson JW and Rice JR (2017) The path-independent M integral implies the creep closure of englacial and subglacial channels. *Journal of Applied Mechanics* **84**(1), 011006. doi: 10.1115/1.4034828

Morlighem M and 9 others (2017) BedMachine v3: Complete bed topography and ocean bathymetry mapping of Greenland from multibeam echo sounding combined with mass conservation. *Geophysical Research Letters* **44**(21), 11–051. doi: 10.1002/2017GL074954

Morlighem M and 31 others (2021) IceBridge BedMachine Greenland, Version 4. *NASA National Snow and Ice Data Center Distributed Active Archive Center*. doi:10.5067/VLJ5YXKCNGXO.

Murray T and Clarke GK (1995) Black-box modeling of the subglacial water system. *Journal of Geophysical Research: Solid Earth* **100**(B6), 10231–10245. doi: 10.1029/95JB00671

Nienow P, Sharp M and Willis I (1998) Seasonal changes in the morphology of the subglacial drainage system, Haut Glacier d'Arolla, Switzerland. *Earth Surface Processes and Landforms: The Journal of the British Geomorphological Group* **23**(9), 825–843. doi: 10.1002/(SICI)1096-9837 (199809)23:9<825::AID-ESP893>3.0.CO;2-2

Oswald G and Gogineni S (2008) Recovery of subglacial water extent from Greenland radar survey data. *Journal of Glaciology* **54**(184), 94–106. doi: 10.3189/002214308784409107

Oswald GK, Rezvanbehbahani S and Stearns LA (2018) Radar evidence of ponded subglacial water in Greenland. *Journal of Glaciology* **64**(247), 711–729. doi: 10.1017/jog.2018.60

Poinar K and 5 others (2017) Drainage of Southeast Greenland firn aquifer water through crevasses to the bed. *Frontiers in Earth Science* **5**, 5. doi: 10.3389/feart.2017.00005

Poinar K, Dow CF and Andrews LC (2019) Long-term support of an active subglacial hydrologic system in Southeast Greenland by firn aquifers. *Geophysical Research Letters* **46**(9), 4772–4781. doi: 10.1029/2019GL082786

Rada C and Schoof C (2018) Channelized, distributed, and disconnected: subglacial drainage under a valley glacier in the Yukon. *The Cryosphere* **12**(8), 2609–2636. doi: 10.5194/tc-12-2609-2018

Rada Giacaman CA and Schoof C (2023) Channelized, distributed, and disconnected: spatial structure and temporal evolution of the subglacial drainage under a valley glacier in the Yukon. *The Cryosphere* **17**(2), 761–787. doi: 10.5194/tc-17-761-2023

Rajaram H, Cheung W and Chaudhuri A (2009) Natural analogs for improved understanding of coupled processes in engineered earth systems: examples from karst system evolution. *Current Science* **97**(8), 1162–1176.

Rempel AW and Meyer CR (2019) Premelting increases the rate of regelation by an order of magnitude. *Journal of Glaciology* **65**(251), 518–521. doi: 10.1017/jog.2019.33

Rempel AW, Meyer CR and Riverman KL (2022) Melting temperature changes during slip across subglacial cavities drive basal mass exchange. *Journal of Glaciology* **68**(267), 197–203. doi: 10.1017/jog.2021.107

Röthlisberger H (1972) Water pressure in intra- and subglacial channels. *Journal of Glaciology* **11**(62), 177–203. doi: 10.3189/S0022143000022188

Ryser C and 7 others (2014a) Caterpillar-like ice motion in the ablation zone of the Greenland ice sheet. *Journal of Geophysical Research: Earth Surface* **119**(10), 2258–2271. doi: 10.1002/2013JF003067

Ryser C and 7 others (2014b) Sustained high basal motion of the Greenland ice sheet revealed by borehole deformation. *Journal of Glaciology* **60**(222), 647–660. doi: 10.3189/2014JoG13J196

Schoof C (2010) Ice-sheet acceleration driven by melt supply variability. *Nature* **468**(7325), 803–806. doi: 10.1038/nature09618

Schoof C, Hewitt IJ and Werder MA (2012) Flotation and free surface flow in a model for subglacial drainage. Part 1. Distributed drainage. *Journal of Fluid Mechanics* **702**, 126–156. doi: 10.1017/jfm.2012.165

Schoof C, Rada C, Wilson N, Flowers G and Haseloff M (2014) Oscillatory subglacial drainage in the absence of surface melt. *The Cryosphere* **8**(3), 959–976. doi: 10.5194/tc-8-959-2014

Shreve R (1972) Movement of water in glaciers. *Journal of Glaciology* **11**(62), 205–214. doi: 10.3189/S002214300002219X

Sommers AN (2018) *Insights into Processes Affecting Greenland Ice Sheet Dynamics in a Changing Climate: Firn Permeability, Interior Thermal State, Subglacial Hydrology, and Heat Transfer Coefficients*. Ph.D. thesis, University of Colorado at Boulder.

Sommers A, Rajaram H and Morlighem M (2018) SHAKTI: Subglacial Hydrology and Kinetic, Transient Interactions v1.0. *Geoscientific Model Development* **11**(7), 2955–2974. doi: 10.5194/gmd-11-2955-2018

Stevens LA and 6 others (2022) Tidewater-glacier response to supraglacial lake drainage. *Nature Communications* **13**(1), 6065. doi: 10.1038/s41467-022-33763-2

Stevens LA, Hewitt IJ, Das SB and Behn MD (2018) Relationship between Greenland Ice Sheet surface speed and modeled effective pressure. *Journal of Geophysical Research: Earth Surface* **123**(9), 2258–2278. doi: 10.1029/2017JF004581

Werder MA, Hewitt IJ, Schoof CG and Flowers GE (2013) Modeling channelized and distributed subglacial drainage in two dimensions. *Journal of Geophysical Research: Earth Surface* **118**(4), 2140–2158. doi: 10.1002/jgrf.20146

Wettlaufer JS and Worster MG (2006) Premelting dynamics. *Annual Review of Fluid Mechanics* **38**(1), 427–452. doi: 10.1146/annurev.fluid.37.061903.175758

Willcocks S, Hasterok D and Jennings S (2021) Thermal refraction: implications for subglacial heat flux. *Journal of Glaciology* **67**(265), 875–884. doi: 10.1017/jog.2021.38

Wright A, Siegert M, Le Brocq A and Gore D (2008) High sensitivity of subglacial hydrological pathways in Antarctica to small ice-sheet changes. *Geophysical Research Letters* **35**(17). doi: 10.1029/2008GL034937

Young TJ and 7 others (2022) Rapid basal melting of the Greenland Ice Sheet from surface meltwater drainage. *Proceedings of the National Academy of Sciences* **119**(10), e2116036119. doi: 10.1073/pnas.2116036119

Zimmerman RW, Al-Yaarubi A, Pain CC and Grattoni CA (2004) Non-linear regimes of fluid flow in rock fractures. *International Journal of Rock Mechanics and Mining Sciences* **41**, 163–169.